nature COMMUNICATIONS

ARTICLE

https://doi.org/10.1038/s41467-022-29002-3 OPEN

Nonlocal pseudopotential energy density functional for orbital-free density functional theory

Qiang Xu[1], Cheng Ma[1], Wenhui Mi[1], Yanchao Wang[1✉] & Yanming Ma[1,2]

Orbital-free density functional theory (OF-DFT) is an electronic structure method with a low computational cost that scales linearly with the number of simulated atoms, making it suitable for large-scale material simulations. It is generally considered that OF-DFT strictly requires the use of local pseudopotentials, rather than orbital-dependent nonlocal pseudopotentials, for the calculation of electron-ion interaction energies, as no orbitals are available. This is unfortunate situation since the nonlocal pseudopotentials are known to give much better transferability and calculation accuracy than local ones. We report here the development of a theoretical scheme that allows the direct use of nonlocal pseudopotentials in OF-DFT. In this scheme, a nonlocal pseudopotential energy density functional is derived by the projection of nonlocal pseudopotential onto the non-interacting density matrix (instead of "orbitals") that can be approximated explicitly as a functional of electron density. Our development defies the belief that nonlocal pseudopotentials are not applicable to OF-DFT, leading to the creation for an alternate theoretical framework of OF-DFT that works superior to the traditional approach.

[1] International Center for Computational Methods and Software & State Key Lab of Superhard Materials, College of Physics, Jilin University, Changchun 130012, China. [2] International Center of Future Science, Jilin University, Changchun 130012, China. ✉email: wyc@calypso.cn

Ab initio calculations using Kohn-Sham (KS) density functional theory (DFT)[1,2] can accurately describe the fundamental properties of various materials. However, its computational cost scales with the cube of the number of electrons in the simulation cell, which poses a major challenge to large-scale simulations. In contrast, orbital-free (OF) DFT is inherent of the lower computational cost that scales linearly with the number of atoms in the system, as it relies only on the electron density and the use of KS orbitals is avoided. As a result, OF-DFT is successfully applied to large-scale simulations of systems with up to millions of atoms[3–6].

The accuracy of OF-DFT simulations depends strongly on the quality of the non-interacting kinetic energy and the electron-ion (or electron-pseudocore) interaction energy employed in the simulations. Many approximate kinetic energy density functionals (KEDFs) have been proposed to evaluate the non-interacting kinetic energy in OF-DFT[7–39]. Their use in combination with local pseudopotentials[40–44] can achieve results that agree reasonably with those derived by KS-DFT, especially for main-group metals, III–V semiconductors[24,34,36,45], and even systems with inhomogeneous electron density such as metal clusters and quantum dots[37,39].

Unfortunately, the local pseudopotentials[28,31,32,40,41,43] used to evaluate the electron-ion interaction energy suffer from a lack of transferability[43], as they fail to reproduce the correct scattering behavior of the all-electron potentials[46–48]. Overcoming the transferability problem requires a reliance on either all-electron potential or nonlocal pseudopotentials (NLPPs), which are widely used in orbital-based approaches. However, it is practically unfeasible to use the all-electron potential, as an accurate all-electron KEDF for OF-DFT calculations is not yet available[49,50]. Furthermore, the use of NLPPs[46,51] runs against conventional understanding, as no orbitals are available in the traditional framework of OF-DFT[41,42,44,52,53].

A crucial nonlocal energy term with a set of angular-momentum-dependent energies has recently been added to OF-DFT calculations[54,55] in an effort to correct errors arising from the use of KEDFs and local pseudopotentials. This approach has successfully reproduced the bulk properties of several standard structures of Ti. However, special care must be taken when applying it to a wide range of practical simulations, as frozen on-site orbitals and empirically directed fitting parameters are part of the model[52]. There is substantial demand for a general approach to evaluate the electron-ion interaction energy using NLPPs in OF-DFT calculations. In this manuscript, we developed a theoretical scheme that allows the direct use of the NLPPs for the calculation of electron-ion interaction energy in OF-DFT, together with a specially designed theoretical framework of OF-DFT. This development leads to an OF-DFT calculation that gives a better transferability than the existing OF-DFT method based on local pseudopotentials.

Results and discussion

Nonlocal pseudopotential energy density functional. In general, the total energy density functional of OF-DFT can be expressed as:

$$E[\rho] = T_s[\rho] + E_H[\rho] + E_{XC}[\rho] + E_{II}\left(\{R_a\}\right) + \int \rho(\mathbf{r}) V_{loc}(\mathbf{r}) d^3\mathbf{r}, \tag{1}$$

where ρ, T_s, E_H, E_{XC}, E_{II}, $\{R_a\}$, and V_{loc} are the electron density, KEDF, Hartree energy, exchange-correlation energy, ion-ion repulsion energy, the set of atomic positions, and local pseudopotential, respectively. To include the nonlocal electron-ion interactions, the total energy density functional of OF-DFT is reformulated as:

$$E[\rho] = T_s[\rho] + E_H[\rho] + E_{XC}[\rho] + E_{II}\left(\{R_a\}\right) + \underbrace{\int \rho(\mathbf{r}) V_{loc}(\mathbf{r}) d^3\mathbf{r} + E_{nl}[\rho]}_{E_{EI}[\rho]}, \tag{2}$$

where the total electron-ion interaction energy $E_{EI}[\rho]$ can be separated into two parts: a local part $E_{loc}[\rho] = \int \rho(\mathbf{r}) V_{loc}(\mathbf{r}) d^3\mathbf{r}$ and a nonlocal part $E_{nl}[\rho]$. All of the terms in Eq. (2) except the nonlocal part of pseudopotential ($E_{nl}[\rho]$) can be evaluated easily.

The exact NLPP energy depends on the KS orbitals or the density matrix:

$$\begin{aligned} E_{nl} &\equiv \sum_i f_i \int\int \psi_i^*(\mathbf{r}') V_{nl}(\mathbf{r}', \mathbf{r}) \psi_i(\mathbf{r}) d^3\mathbf{r} d^3\mathbf{r}' \\ &= \int\int V_{nl}(\mathbf{r}', \mathbf{r}) \gamma_s(\mathbf{r}, \mathbf{r}') d^3\mathbf{r} d^3\mathbf{r}', \end{aligned} \tag{3}$$

where f_i, $V_{nl}(\mathbf{r}', \mathbf{r}) = \langle \mathbf{r}' | \hat{V}_{nl} | \mathbf{r} \rangle$, and $\gamma_s(\mathbf{r}, \mathbf{r}') = \sum_i f_i \psi_i(\mathbf{r}) \psi_i^*(\mathbf{r}')$ represent the occupation number of the ith KS orbital ψ_i, the real-space representation of the nonlocal part pseudopotential, and the non-interacting density matrix, respectively. Considering that the density matrices $\gamma_s[\rho](\mathbf{r}, \mathbf{r}')$ can be used to approximate the KEDFs[7,56,57], an NLPP energy density functional (NLPPF) relying directly on the density matrix is proposed to evaluate the nonlocal electron-ion interaction energy. The nonlocal electron-ion interaction energy is then rewritten as a function of electron density

$$E_{nl}[\rho] = \int\int V_{nl}(\mathbf{r}', \mathbf{r}) \gamma_s[\rho](\mathbf{r}, \mathbf{r}') d^3\mathbf{r} d^3\mathbf{r}'. \tag{4}$$

By taking the Kleinman-Bylander form[58] of norm-conserving NLPPs, the nonlocal part pseudopotential[59] can be written as

$$V_{nl}(\mathbf{r}', \mathbf{r}) = \sum_{a,lm} E_{KB}^{a,lm} \chi_{lm}^a(\mathbf{r}') \chi_{lm}^{a*}(\mathbf{r}), \tag{5}$$

where $E_{KB}^{a,lm} = \left[\int \phi_{lm}^{a*}(\mathbf{r}) \delta V_l^a(\mathbf{r}) \phi_{lm}^a(\mathbf{r}) d^3\mathbf{r}\right]^{-1}$ and $\chi_{lm}^a(\mathbf{r}) = \delta V_l^a(\mathbf{r}) \phi_{lm}^a(\mathbf{r})$. The terms ϕ_{lm}^a and δV_l^a are the atomic pseudo-wavefunction and the short-range pseudopotential corresponding to the lmth angular momentum of ath atom, respectively. $\gamma_s[\rho]$ denotes the density matrix as a function of electron distribution ρ. Although there is no exact analytic form available for the density matrix functional, a modified Gaussian (MG)[60] form derived from the second-order Taylor expansions of the density matrix[61] was employed to approximate the density matrix functional:

$$\gamma_s^{MG}[\rho](\mathbf{r}, \mathbf{r}') = \rho(\bar{\mathbf{r}}) e^{-\frac{s^2}{2\beta(\bar{\mathbf{r}})}} \left[1 + A\left(\frac{s^2}{2\beta(\bar{\mathbf{r}})}\right)^2\right], \tag{6}$$

where $s = |\mathbf{r} - \mathbf{r}'|$ and $\bar{\mathbf{r}} = (\mathbf{r} + \mathbf{r}')/2$. The second term in the square bracket is $O(s^4)$ correction[60], where A is an adjustable parameter. $\beta(\mathbf{r})$ denotes the "local temperature" $\beta(\mathbf{r}) = \frac{3}{2}\frac{\rho(\mathbf{r})}{t_s(\mathbf{r})}$[62,63], where $t_s(\mathbf{r})$ is the exact kinetic energy density defined as $t_s(\mathbf{r}) = t_s^{KS}(\mathbf{r}) \equiv \sum_{i=1}^{Occ.} \frac{1}{8} |\nabla \rho_i(\mathbf{r})|^2 / \rho_i(\mathbf{r}) - \frac{1}{8} \nabla^2 \rho(\mathbf{r})$ and $\rho_i(\mathbf{r}) = |\psi_i(\mathbf{r})|^2$ is ith KS orbital's density (see Refs. [60,61]). To remove the orbital-dependent problem in $t_s(\mathbf{r})$ and obtain a solely density-dependent form of the density matrix functional, the kinetic energy density is obtained directly from the integrand of KEDFs to replace the exact one: $t_s(\mathbf{r}) \approx t_s[\rho](\mathbf{r})$. The widely used Wang-Teter (WT) KEDF[28] is chosen as an exemplary case, and $t_s[\rho](\mathbf{r})$ can be

expressed as

$$t_s^{WT}[\rho](\mathbf{r}) = \frac{3}{10}\left(3\pi^2\right)^{2/3}\rho^{5/3}(\mathbf{r}) + \frac{1}{8}\frac{\left|\nabla\rho(\mathbf{r})\right|^2}{\rho(\mathbf{r})} + \rho^{5/6}(\mathbf{r})\int \omega_{WT}(\mathbf{r},\mathbf{r}')\rho^{5/6}(\mathbf{r}')d^3\mathbf{r}', \quad (7)$$

where $\omega_{WT}(\mathbf{r},\mathbf{r}')$ is the kernel of WT functional. The Supplementary Notes give the details of the kinetic energy densities obtained from WT and Xu-Wang-Ma[38] KEDFs.

The direct numerical evaluations of $\rho(\bar{\mathbf{r}})$ and $\beta(\bar{\mathbf{r}})$ at the average position $\bar{\mathbf{r}}$ are very complicated. They are therefore approximated using q-mean "nonlocal density" $\rho_q(\mathbf{r},\mathbf{r}') = \left[\frac{\rho^q(\mathbf{r})+\rho^q(\mathbf{r}')}{2}\right]^{1/q}$ and two-point average temperature $\beta(\mathbf{r},\mathbf{r}') = [\beta(\mathbf{r})+\beta(\mathbf{r}')]/2$ for systems with slowly varying electron densities. The density matrix functional of Eq. (6) can then be reformulated as

$$\tilde{\gamma}_s^{MG}[\rho](\mathbf{r},\mathbf{r}') = \rho_q(\mathbf{r},\mathbf{r}')e^{-\frac{s^2}{2\beta(\mathbf{r},\mathbf{r}')}}\left[1 + A\left(\frac{s^2}{2\beta(\mathbf{r},\mathbf{r}')}\right)^2\right]. \quad (8)$$

Combining Eqs. (4), (5), and (8) gives the NLPPF as

$$E_{nl}[\rho] \approx \sum_{a,lm} E_{KB}^{a,lm}\int_{\Omega_a}\int_{\Omega_a}\chi_{lm}^{a}(\mathbf{r}')\chi_{lm}^{a*}(\mathbf{r})\tilde{\gamma}_s^{MG}[\rho](\mathbf{r},\mathbf{r}')d^3\mathbf{r}d^3\mathbf{r}', \quad (9)$$

where the integral domain Ω_a is the ath ionic core region. Owing to the short-range nature of $\{\chi_{lm}^a(\mathbf{r})\}$, the computational cost of Eq. (9) scales linearly $\mathcal{O}[cN_a]$ with the number of atoms (N_a), where c can be regarded as a constant derived from the double integral within the near-core region. Within the NLPPF scheme, a new theoretical framework of OF-DFT has been built and implemented in ATLAS[5,64]. The further computational details are provided in Methods Section. The parameters of pseudopotential and NLPPF are presented in Supplementary Tables 1 and 2, respectively.

Computational accuracy of NLPPF scheme. We first applied this scheme for OF-DFT calculations of Li, Mg, and Cs within hexagonal-close-packed (HCP), face-centered cubic (FCC), body-centered cubic (BCC), simple cubic (SC), and cubic diamond structures. For each structure, 13 energy-volume points were calculated by expanding and compressing the approximate equilibrium volume by up to 20%, and the bulk properties (the equilibrium cell volume V_0, bulk modulus B_0, and the relative energy E_R with respect to HCP structure) were determined by fitting the energy-volume curve against Murnaghan's equation of state[65]. The comparison of the results obtained by OF-DFT using both local pseudopotentials (BLPS[41] and OEPP[43]) and NLPPs against those calculated by KS-DFT using the projector augmented-wave (PAW)[66] method are presented in Supplementary Table 3. For Li and Mg solids, the OF-DFT calculations within both local pseudopotentials and NLPPs give reasonable predictions of V_0, B_0, and E_R, which are comparable with the KS-DFT results. It is noteworthy that our scheme shows an improvement over the local pseudopotentials of OEPP for bulk Cs. The accurate bulk properties of Li/Mg/Cs obtained by the current scheme demonstrate its valid applicability to simple metallic solids.

Further assessment of the accuracy of our scheme was demonstrated by molecular dynamics calculations for Li-Mg alloy. The calculations used a canonical ensemble (at 1000 K) in a supercell containing 108 atoms ($Li_{54}Mg_{54}$). The calculated pair distribution functions $g(r)$ for Li-Mg alloy are shown in Fig. 1. Overall, the predicted shapes and peak neighbors of pair distribution functions by OF-DFT within NLPPF match the

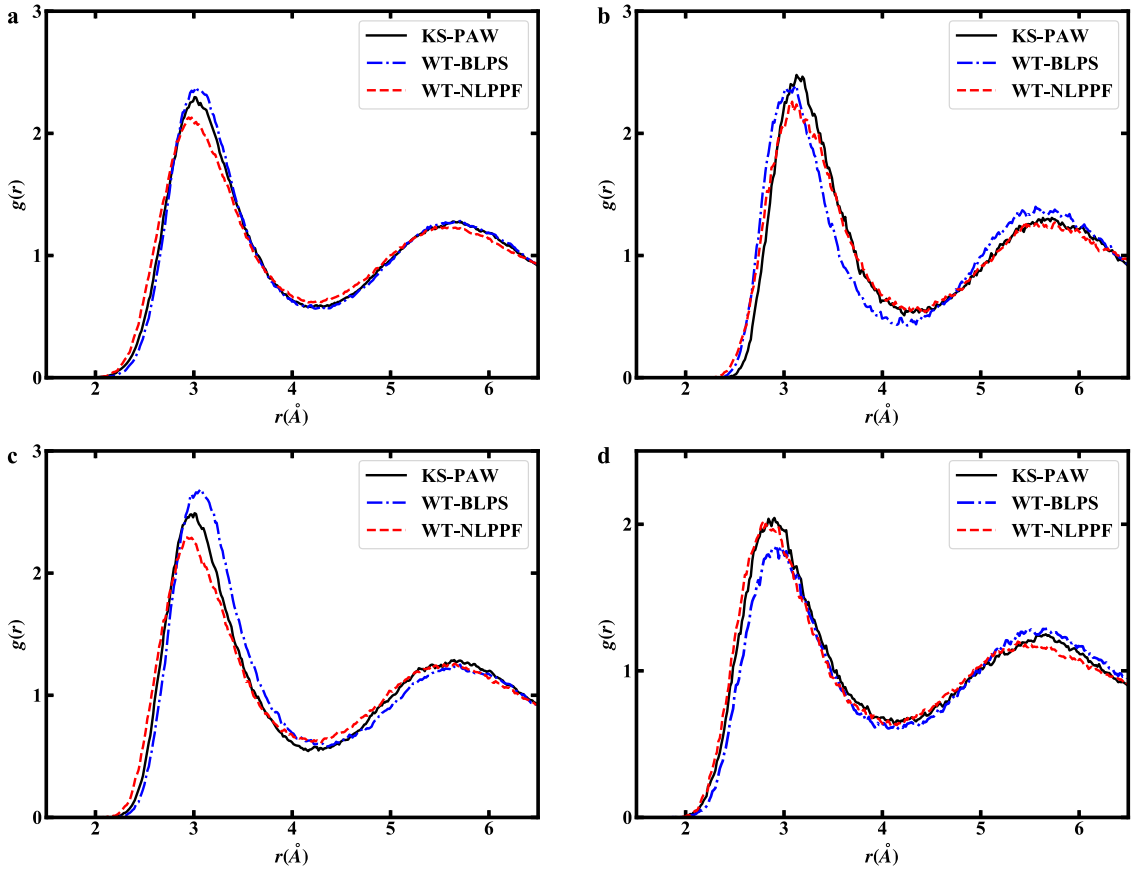

Fig. 1 Pair distribution functions for $Li_{54}Mg_{54}$ alloy. a Total, **b** Mg-Mg, **c** Li-Mg, and **d** Li-Li pair distribution functions.

results calculated by KS-DFT. Especially notable are the resulting contributions of the partial distributions (Fig. 1b–d) calculated by OF-DFT within the NLPPF being almost identical to the KS-DFT calculations, which are superior to those obtained by the local pseudopotentials.

Transferability of NLPPF scheme. To demonstrate the transferability of our scheme, we randomly generated 50 structures of Li systems using CALYPSO[67,68]. The total energies of these structures were calculated by OF-DFT and KS-DFT. The comparisons of total energy relative to the HCP structure (E_R) are shown in Fig. 2. The orderings of energy are well captured by OF-DFT within NLPPF. The relative energies of different phases are overall well reproduced and in reasonable agreement with the KS-DFT results. The least-square fitting lines of WT-NLPPF are generally closer to the KS-PAW results than those from the local pseudopotentials. For example, the mean error of E_R for Li systems obtained by OF-DFT within the WT-NLPPF is 45 meV/atom, which is lower than that within BLPS (73 meV/atom), or OEPP (201 meV/atom). Therefore, this framework of OF-DFT with improved transferability is superior to the traditional one.

Previous studies have shown that OF-DFT with local pseudopotentials can be applied to most *s*- and *p*-block metals. However, OF-DFT simulation using the local pseudopotential OEPP shows unacceptable errors for various crystalline phases of Be (Fig. 3): the curves of energy with respect to volume for HCP and FCC structures show the total energy monotonically decreasing with increasing volume. In contrast, the curves with clear minima predicted by OF-DFT within NLPPF agree well with those produced by KS-DFT. These findings indicate the significant superiority of our proposed framework over the conventional one.

Note that the bulk properties (e.g., equilibrium volume, bulk modulus, and relative energy) calculated by OF-DFT within NLPPF reproduce the results of KS-DFT for Li and Mg almost exactly (Table 1), considering the maximal deviation of E_R is within 32 meV/atom. However, there are some discrepancies for crystalline phases of Be: in particular, the deviation of E_R for the SC structure is larger than 400 meV/atom. To explore the causes of these discrepancies, we estimated the errors of the kinetic energy density of the WT-KEDF with respect to the KS kinetic energy density along the [100] and [111] directions in the SC structures of Li, Mg, and Be (Fig. 4). The kinetic energy density of KS-DFT is clearly reproduced accurately by the WT-KEDF for Li and Mg with slow variations of electron densities. However, it is seriously underestimated for Be, in which the electron distribution rapidly varies in the near-core region. Therefore, we believe that errors in the kinetic energy densities for Be lead to the discrepancy in its bulk properties obtained by the framework of

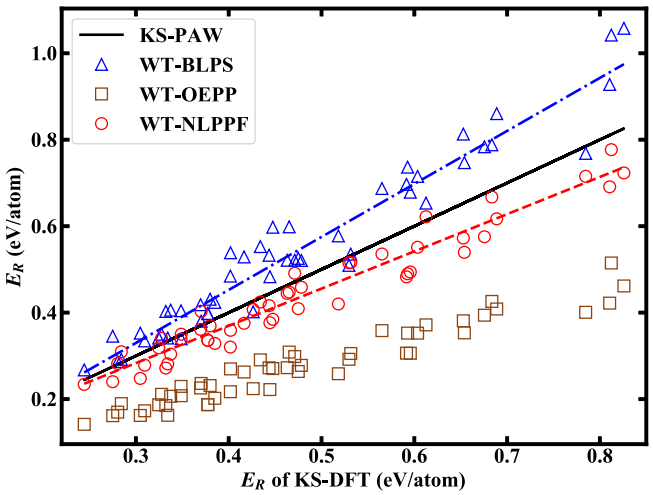

Fig. 2 Relative energies for random structures of elemental Li. The results are calculated by OF-DFT using BLPS, OEPP and NLPPF in comparison with that by KS-DFT using the PAW method. Blue dash-dotted and red dashed lines are the least-square fittings of WT-BLPS and WT-NLPPF results, respectively.

Table 1 B_0 (GPa), E_R (eV/atom), and V_0 (Å^3/atom) for bulk Li, Mg, and Be by KS-DFT and OF-DFT.

		Method	HCP	FCC	BCC	SC
Li	B_0	KS-PAW	13.9	13.6	13.9	12.1
		WT-NLPPF	13.5	13.5	13.7	11.0
	V_0	KS-PAW	20.280	20.372	20.396	20.580
		WT-NLPPF	19.483	19.462	19.352	20.844
	E_R	KS-PAW	0.000	0.000	0.001	0.120
		WT-NLPPF	0.000	0.000	0.001	0.152
Mg	B_0	KS-PAW	35.8	35.5	34.8	22.7
		WT-NLPPF	33.0	31.3	31.3	21.2
	V_0	KS-PAW	22.838	23.071	22.826	27.478
		WT-NLPPF	23.194	23.924	23.730	28.274
	E_R	KS-PAW	0.000	0.012	0.029	0.382
		WT-NLPPF	0.000	0.011	0.031	0.372
Be	B_0	KS-PAW	123.3	119.7	124.1	74.5
		WT-NLPPF	91.5	90.5	87.2	63.3
	V_0	KS-PAW	7.910	7.875	7.822	10.274
		WT-NLPPF	7.690	7.942	7.798	10.160
	E_R	KS-PAW	0.000	0.080	0.099	1.004
		WT-NLPPF	0.000	0.058	0.082	0.561

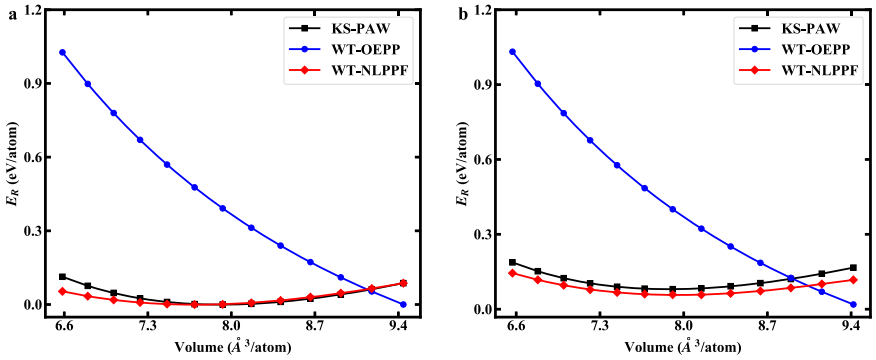

Fig. 3 Relative energy versus volume curves for Be systems. a The calculated energy-volume curves of Be-HCP. **b** The calculated energy-volume curves of Be-FCC. The total energy shift of WT-OEPP is −33.030 eV/atom.

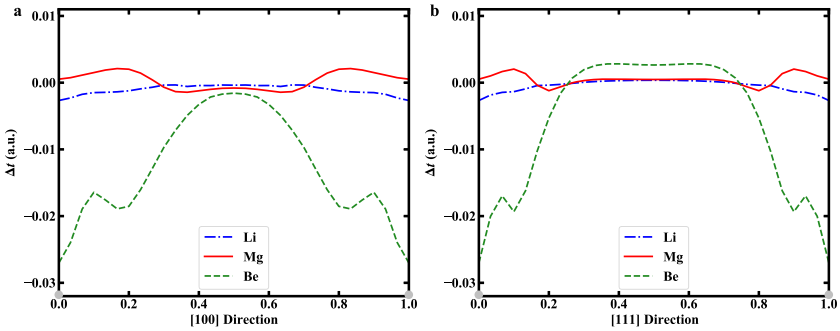

Fig. 4 Kinetic energy differences in SC structure for Li, Mg, and Be systems. a The calculated differences along [100] direction. **b** The calculated differences along [111] direction. Note that $\Delta t(\mathbf{r}) \equiv t_s^{WT}[\rho^{KS}](\mathbf{r}) - t_s^{KS}(\mathbf{r})$.

Table 2 B_0 (GPa), E_R (eV/atom), and V_0 (Å^3/atom) for bulk Cd by KS-DFT and OF-DFT.

		Method	HCP	FCC	BCC	SC
Cd	B_0	KS-PAW	40.8	41.0	34.5	29.2
		KS-NLPP	67.4	66.2	66.1	39.8
		WT-OEPP	148.2	138.8	147.1	74.8
		WT-NLPPF	67.0	64.8	65.2	39.8
	V_0	KS-PAW	22.758	22.979	23.512	27.141
		KS-NLPP	15.684	15.851	15.674	18.487
		WT-OEPP	10.379	10.693	10.379	11.964
		WT-NLPPF	15.702	16.027	15.763	18.878
	E_R	KS-PAW	0.000	0.004	0.053	0.121
		KS-NLPP	0.000	0.019	0.036	0.436
		WT-OEPP	0.000	0.138	0.072	0.979
		WT-NLPPF	0.000	0.036	0.056	0.451

OF-DFT within the NLPPF. The findings are fairly consistent with our expectation that the performance of the NLPPF relies strongly on the accuracy of kinetic energy density, as manifested by Eqs. (7) and (8).

Due to the existence of significant differences in kinetic energy density between WT and the exact one for Cd systems including localized *d*-channel electrons (see Supplementary Fig. 1), the NLPPF using WT cannot be applicable to investigate Cd systems with *d*-channel electrons. Therefore, the NLPP of Cd was constructed without *d*-channel electrons for the additional calculations. As listed in Table 2, the bulk properties predicted by the OF-DFT within NLPPF framework agree fairly well with the predictions by KS-DFT using the same NLPP, whereas WT-OEPP gives serious discrepancies compared with KS-NLPP results in all bulk properties. Although the calculations using NLPP without *d*-channel electrons cannot give the accurate bulk properties for Cd systems (Table 2), OF-DFT within NLPPF works superior to that within OEPP. Overall, it can be expected this NLPPF scheme using accurate KEDF and its kinetic energy density can be applied to the systems including localized electrons, such as the transition metals or covalent systems.

Computational efficiency of NLPPF scheme. To assess the computational efficiency of the current scheme, static simulations of Cs BCC supercells containing 128–16,000 atoms were performed by OF-DFT within NLPPF. The total wall time of the single point energy calculations is plotted with respect to the number of atoms in Supplementary Fig. 2. The computational cost of this framework clearly scales linearly with the number of atoms in the simulation cell, in sharp contrast to the cubic scaling of KS-DFT. This shows that the OF-DFT within NLPPF is potentially applicable to the simulation of large-scale systems containing millions of atoms.

In summary, we proposed an NLPPF scheme that allows the direct use of NLPPs in OF-DFT calculations. The static and dynamic properties of *s*- and *p*-block metals calculated within this scheme agree well with KS-DFT predictions and show significant improvements in the computational accuracy and transferability over conventional OF-DFT with local pseudopotentials. With this work, we defy the conventional wisdom of orbital-dependent NLPPs being incompatible with OF-DFT, leading to the creation of an alternative framework of OF-DFT, which opens up new avenues for further development of the theory.

Methods

Pseudopotential generations. The Troullier-Martins NLPPs[59] are generated by the FHI98PP[47] code for all considered systems [see Supplementary Table 1] and the *p*-channel of the NLPPs is used as the local pseudopotential of $V_{loc}(r)$ in OF-DFT.

Numerical calculations. The KS-DFT calculations using the PAW[66] and NLPP are performed by VASP[69,70] and ARES packages[71], respectively. The k-point meshes are generated using the Monkhorst-Pack method[72] with the k-spacing of 0.10 Å^{-1}. The kinetic energy cutoff is 500 eV for all the simulations using VASP. The OF-DFT calculations are carried out by ATLAS[5,64] using WT[28] as KEDF, and the corresponding kinetic energy density is used to construct the NLPPF. The generalized gradient approximation with the form of Perdew-Burke-Ernzerhof[73] is employed for both OF-DFT and KS-DFT calculations. The grid spacings of 0.18, 0.18, 0.22, 0.10, 0.15, 0.22, 0.12, and 0.15 Å are used in ATLAS/ARES for Li, Mg, Cs, Be, Cd, K, Zn, and Li-Mg alloy, respectively. The parameters of *A* and *q* in NLPPFs are presented in Supplementary Table 2 carefully tuned to yield the bulk properties, which agree with the KS-DFT (NLPPs) predictions.

Molecular dynamics. The molecular dynamic simulations of Li-Mg alloy are performed in the canonical ensemble (at 1000 K) applying the Nosé-Hoover thermostat[74,75] simulations up to 10 ps (0.5 fs/step), with the first 10,000 steps for equilibrating the system. The data for further analysis were collected from the subsequent 10,000 steps.

Data availability

The authors declare that the main data supporting the findings of this study are contained within the paper and its associated Supplementary Information. All other relevant data are available from the corresponding authors upon reasonable request.

Received: 11 January 2022; Accepted: 22 February 2022;
Published online: 16 March 2022

References

1. Hohenberg, P. & Kohn, W. Inhomogeneous electron gas. *Phys. Rev.* **136**, B864 (1964).
2. Kohn, W. & Sham, L. J. Self-consistent equations including exchange and correlation effects. *Phys. Rev.* **140**, A1133 (1965).

3. Chen, M. et al. Introducing profess 3.0: an advanced program for orbital-free density functional theory molecular dynamics simulations. *Computer Phys. Commun.* **190**, 228–230 (2015).
4. Chen, M., Jiang, X.-W., Zhuang, H., Wang, L.-W. & Carter, E. A. Petascale orbital-free density functional theory enabled by small-box algorithms. *J. Chem. Theory Comput.* **12**, 2950–2963 (2016).
5. Shao, X. et al. Large-scale ab initio simulations for periodic system. *Computer Phys. Commun.* **233**, 78–83 (2018).
6. Shao, X., Jiang, K., Mi, W., Genova, A. & Pavanello, M. Dftpy: an efficient and object-oriented platform for orbital-free DTF simulations. *Wiley Interdiscip. Rev.: Computational Mol. Sci.* **11**, e1482 (2021).
7. Wang, Y. A. & Carter, E. A. *Orbital-Free Kinetic-Energy Density Functional Theory*, 117–184 (Springer Netherlands, Dordrecht, 2002).
8. Wesolowski, T. A. & Wang, Y. A. *Recent Progress in Orbital-free Density Functional Theory* (World Scientific, 2013).
9. Thomas, L. H. The calculation of atomic fields. *Math. Proc. Camb. Philos. Soc.* **23**, 542–548 (1927).
10. Fermi, E. Statistical method to determine some properties of atoms. *Rend. Accad. Naz. Lincei* **6**, 5 (1927).
11. Fermi, E. Eine statistische methode zur bestimmung einiger eigenschaften des atoms und ihre anwendung auf die theorie des periodischen systems der elemente. *Z. f.ür. Phys.* **48**, 73–79 (1928).
12. Weizsäcker, C. V. Zur theorie der kernmassen. *Z. f.ür. Phys.* **96**, 431–458 (1935).
13. Ou-Yang, H. & Levy, M. Theorem for functional derivatives in density-functional theory. *Phys. Rev. A* **44**, 54 (1991).
14. Perdew, J. P. Generalized gradient approximation for the fermion kinetic energy as a functional of the density. *Phys. Lett. A* **165**, 79–82 (1992).
15. Thakkar, A. J. Comparison of kinetic-energy density functionals. *Phys. Rev. A* **46**, 6920 (1992).
16. Vitos, L., Johansson, B., Kollar, J. & Skriver, H. L. Local kinetic-energy density of the airy gas. *Phys. Rev. A* **61**, 052511 (2000).
17. Ernzerhof, M. The role of the kinetic energy density in approximations to the exchange energy. *J. Mol. Structure: THEOCHEM* **501**, 59–64 (2000).
18. García-Aldea, D. & Alvarellos, J. Kinetic energy density study of some representative semilocal kinetic energy functionals. *J. Chem. Phys.* **127**, 144109 (2007).
19. Constantin, L. A. & Ruzsinszky, A. Kinetic energy density functionals from the airy gas with an application to the atomization kinetic energies of molecules. *Phys. Rev. B* **79**, 115117 (2009).
20. Constantin, L. A., Fabiano, E., Laricchia, S. & Della Sala, F. Semiclassical neutral atom as a reference system in density functional theory. *Phys. Rev. Lett.* **106**, 186406 (2011).
21. Laricchia, S., Fabiano, E., Constantin, L. & Della Sala, F. Generalized gradient approximations of the noninteracting kinetic energy from the semiclassical atom theory: rationalization of the accuracy of the frozen density embedding theory for nonbonded interactions. *J. Chem. Theory Comput.* **7**, 2439–2451 (2011).
22. Karasiev, V. V., Chakraborty, D., Shukruto, O. A. & Trickey, S. Nonempirical generalized gradient approximation free-energy functional for orbital-free simulations. *Phys. Rev. B* **88**, 161108 (2013).
23. Constantin, L. A., Fabiano, E., Śmiga, S. & Della Sala, F. Jellium-with-gap model applied to semilocal kinetic functionals. *Phys. Rev. B* **95**, 115153 (2017).
24. Luo, K., Karasiev, V. V. & Trickey, S. A simple generalized gradient approximation for the noninteracting kinetic energy density functional. *Phys. Rev. B* **98**, 041111 (2018).
25. Constantin, L. A., Fabiano, E. & Della Sala, F. Semilocal Pauli–Gaussian kinetic functionals for orbital-free density functional theory calculations of solids. *J. Phys. Chem. Lett.* **9**, 4385–4390 (2018).
26. Luo, K., Karasiev, V. V. & Trickey, S. Towards accurate orbital-free simulations: a generalized gradient approximation for the noninteracting free energy density functional. *Phys. Rev. B* **101**, 075116 (2020).
27. Chacón, E., Alvarellos, J. & Tarazona, P. Nonlocal kinetic energy functional for nonhomogeneous electron systems. *Phys. Rev. B* **32**, 7868 (1985).
28. Wang, L.-W. & Teter, M. P. Kinetic-energy functional of the electron density. *Phys. Rev. B* **45**, 13196 (1992).
29. Smargiassi, E. & Madden, P. A. Orbital-free kinetic-energy functionals for first-principles molecular dynamics. *Phys. Rev. B* **49**, 5220 (1994).
30. Perrot, F. Hydrogen-hydrogen interaction in an electron gas. *J. Phys.: Condens. Matter* **6**, 431 (1994).
31. Wang, Y. A., Govind, N. & Carter, E. A. Orbital-free kinetic-energy functionals for the nearly free electron gas. *Phys. Rev. B* **58**, 13465 (1998).
32. Wang, Y. A., Govind, N. & Carter, E. A. Orbital-free kinetic-energy density functionals with a density-dependent kernel. *Phys. Rev. B* **60**, 16350 (1999).
33. Garcia-Aldea, D. & Alvarellos, J. Kinetic-energy density functionals with nonlocal terms with the structure of the thomas-fermi functional. *Phys. Rev. A* **76**, 052504 (2007).
34. Huang, C. & Carter, E. A. Nonlocal orbital-free kinetic energy density functional for semiconductors. *Phys. Rev. B* **81**, 045206 (2010).
35. Constantin, L. A., Fabiano, E. & Della Sala, F. Nonlocal kinetic energy functional from the jellium-with-gap model: applications to orbital-free density functional theory. *Phys. Rev. B* **97**, 205137 (2018).
36. Mi, W., Genova, A. & Pavanello, M. Nonlocal kinetic energy functionals by functional integration. *J. Chem. Phys.* **148**, 184107 (2018).
37. Mi, W. & Pavanello, M. Orbital-free density functional theory correctly models quantum dots when asymptotics, nonlocality, and nonhomogeneity are accounted for. *Phys. Rev. B* **100**, 041105 (2019).
38. Xu, Q., Wang, Y. & Ma, Y. Nonlocal kinetic energy density functional via line integrals and its application to orbital-free density functional theory. *Phys. Rev. B* **100**, 205132 (2019).
39. Xu, Q., Lv, J., Wang, Y. & Ma, Y. Nonlocal kinetic energy density functionals for isolated systems obtained via local density approximation kernels. *Phys. Rev. B* **101**, 045110 (2020).
40. Zhou, B., Wang, Y. A. & Carter, E. A. Transferable local pseudopotentials derived via inversion of the Kohn-Sham equations in a bulk environment. *Phys. Rev. B* **69**, 125109 (2004).
41. Huang, C. & Carter, E. A. Transferable local pseudopotentials for magnesium, aluminum and silicon. *Phys. Chem. Chem. Phys.* **10**, 7109–7120 (2008).
42. del Rio, B. G. & Gonzalez, L. E. Orbital free ab initio simulations of liquid alkaline earth metals: from pseudopotential construction to structural and dynamic properties. *J. Phys.: Condens. Matter* **26**, 465102 (2014).
43. Mi, W., Zhang, S., Wang, Y., Ma, Y. & Miao, M. First-principle optimal local pseudopotentials construction via optimized effective potential method. *J. Chem. Phys.* **144**, 134108 (2016).
44. Del Rio, B. G., Dieterich, J. M. & Carter, E. A. Globally-optimized local pseudopotentials for (orbital-free) density functional theory simulations of liquids and solids. *J. Chem. Theory Comput.* **13**, 3684–3695 (2017).
45. Shao, X., Mi, W. & Pavanello, M. Revised huang-carter nonlocal kinetic energy functional for semiconductors and their surfaces. *Phys. Rev. B* **104**, 045118 (2021).
46. Hamann, D., Schlüter, M. & Chiang, C. Norm-conserving pseudopotentials. *Phys. Rev. Lett.* **43**, 1494 (1979).
47. Fuchs, M. & Scheffler, M. Ab initio pseudopotentials for electronic structure calculations of poly-atomic systems using density-functional theory. *Computer Phys. Commun.* **119**, 67–98 (1999).
48. Martin, R. M. *Electronic Structure: Basic Theory and Practical Methods* (Cambridge University Press, 2004).
49. Lehtomäki, J., Makkonen, I., Caro, M. A., Harju, A. & Lopez-Acevedo, O. Orbital-free density functional theory implementation with the projector augmented-wave method. *J. Chem. Phys.* **141**, 234102 (2014).
50. Zavodinsky, V. & Gorkusha, O. A. On a possibility to develop a full-potential orbital-free modeling approach. *Nanosystems: Phys., Chem., Math.* **10**, 402–409 (2019).
51. Vanderbilt, D. Soft self-consistent pseudopotentials in a generalized eigenvalue formalism. *Phys. Rev. B* **41**, 7892 (1990).
52. Witt, W. C., Del Rio, B. G., Dieterich, J. M. & Carter, E. A. Orbital-free density functional theory for materials research. *J. Mater. Res.* **33**, 777 (2018).
53. Witt, W. C., Shires, B. W., Tan, C. W., Jankowski, W. J. & Pickard, C. J. Random structure searching with orbital-free density functional theory. *J. Phys. Chem. A* **125**, 1650–1660 (2021).
54. Ke, Y., Libisch, F., Xia, J., Wang, L.-W. & Carter, E. A. Angular-momentum-dependent orbital-free density functional theory. *Phys. Rev. Lett.* **111**, 066402 (2013).
55. Ke, Y., Libisch, F., Xia, J. & Carter, E. A. Angular momentum dependent orbital-free density functional theory: formulation and implementation. *Phys. Rev. B* **89**, 155112 (2014).
56. Chakraborty, D., Cuevas-Saavedra, R. & Ayers, P. W. Two-point weighted density approximations for the kinetic energy density functional. *Theor. Chem. Acc.* **136**, 1–12 (2017).
57. Chakraborty, D., Cuevas-Saavedra, R. & Ayers, P. W. *Kinetic Energy Density Functionals from Models for the One-Electron Reduced Density Matrix*, 199–208 (Springer International Publishing, Cham, 2018).
58. Kleinman, L. & Bylander, D. Efficacious form for model pseudopotentials. *Phys. Rev. Lett.* **48**, 1425 (1982).
59. Troullier, N. & Martins, J. L. Efficient pseudopotentials for plane-wave calculations. *Phys. Rev. B* **43**, 1993 (1991).
60. Lee, C. & Parr, R. G. Gaussian and other approximations to the first-order density matrix of electronic systems, and the derivation of various local-density-functional theories. *Phys. Rev. A* **35**, 2377 (1987).
61. Berkowitz, M. Exponential approximation for the density matrix and the Wigner's distribution. *Chem. Phys. Lett.* **129**, 486–488 (1986).
62. Parr, R. G. & Yang, W. *Density-Functional Theory of Atoms and Molecules*. (Oxford University Press, New York, 1989).

63. Ghosh, S. K., Berkowitz, M. & Parr, R. G. Transcription of ground-state density-functional theory into a local thermodynamics. *Proc. Natl Acad. Sci. USA.* **81**, 8028–8031 (1984).
64. Mi, W. et al. Atlas: a real-space finite-difference implementation of orbital-free density functional theory. *Computer Phys. Commun.* **200**, 87–95 (2016).
65. Murnaghan, F. The volume changes of five gases under high pressures. *J. Frankl. Inst.* **197**, 98 (1924).
66. Blöchl, P. E. Projector augmented-wave method. *Phys. Rev. B* **50**, 17953 (1994).
67. Wang, Y., Lv, J., Zhu, L. & Ma, Y. Crystal structure prediction via particle-swarm optimization. *Phys. Rev. B* **82**, 094116 (2010).
68. Wang, Y., Lv, J., Zhu, L. & Ma, Y. Calypso: a method for crystal structure prediction. *Computer Phys. Commun.* **183**, 2063–2070 (2012).
69. Kresse, G. & Furthmüller, J. Efficient iterative schemes for ab initio total-energy calculations using a plane-wave basis set. *Phys. Rev. B* **54**, 11169 (1996).
70. Kresse, G. & Furthmüller, J. Efficiency of ab-initio total energy calculations for metals and semiconductors using a plane-wave basis set. *Computational Mater. Sci.* **6**, 15–50 (1996).
71. Xu, Q. et al. Ab initio electronic structure calculations using a real-space Chebyshev-filtered subspace iteration method. *J. Phys.: Condens. Matter* **31**, 455901 (2019).
72. Monkhorst, H. J. & Pack, J. D. Special points for Brillouin-zone integrations. *Phys. Rev. B* **13**, 5188 (1976).
73. Perdew, J. P., Burke, K. & Ernzerhof, M. Generalized gradient approximation made simple. *Phys. Rev. Lett.* **77**, 3865 (1996).
74. Nosé, S. A unified formulation of the constant temperature molecular dynamics methods. *J. Chem. Phys.* **81**, 511–519 (1984).
75. Hoover, W. G. Canonical dynamics: equilibrium phase-space distributions. *Phys. Rev. A* **31**, 1695–1697 (1985).

Acknowledgements

Q.X., Y.W., and Y.M. acknowledge funding support from the National Natural Science Foundation of China under Grants No. 12047530, 12034009, 91961204, 11774127, 12174142, 11404128, 11822404, and 11974134; the Program for JLU Science and Technology Innovative Research Team. Part of the calculation was performed in the high-performance computing center of Jilin University.

Author contributions

Q.X., Y.W., and Y.M. conceived and designed the project and theoretical framework. Q.X. and C.M. implemented the computational code for this framework in the ATLAS package and performed the computer simulations. Q.X., W.M., Y.W., and Y.M. analyzed the results and wrote the manuscripts. All authors contributed to the discussion and revision of the manuscript.

Competing interests

The authors declare no competing interests.

Additional information

Supplementary information The online version contains supplementary material available at https://doi.org/10.1038/s41467-022-29002-3.

Correspondence and requests for materials should be addressed to Yanchao Wang.

Peer review information *Nature Communications* thanks the anonymous reviewers for their contribution to the peer review of this work.

Reprints and permission information is available at http://www.nature.com/reprints

Publisher's note Springer Nature remains neutral with regard to jurisdictional claims in published maps and institutional affiliations.